# Comparison and Validation of Acoustic Response Models for Wind Noise Reduction Pipe Arrays

JULIEN MARTY

CTBTO, Vienna, Austria

STÉPHANE DENIS

CEA, DAM, DIF, Arpajon, France

## THOMAS GABRIELSON

Applied Research Laboratory, The Pennsylvania State University, University Park, Pennsylvania

## MILTON GARCÉS

Infrasound Laboratory, University of Hawai'i at Mānoa, Kailua-Kona, Hawaii

### DAVID BROWN

CTBTO, Vienna, Austria

(Manuscript received 7 June 2016, in final form 13 September 2016)

## ABSTRACT

The detection capability of the infrasound component of the International Monitoring System (IMS) is tightly linked to the performance of its wind noise reduction systems. The wind noise reduction solution implemented at all IMS infrasound measurement systems consists of a spatial distribution of air inlets connected to the infrasound sensor through a network of pipes. This system, usually referred to as "pipe array," has proven its efficiency in operational conditions. The objective of this paper is to present the results of the comparison and validation of three distinct acoustic response models for pipe arrays. The characteristics of the models and the results obtained for a defined set of pipe array configurations are described. A field experiment using a newly developed infrasound generator, dedicated to the validation of these models, is then presented. The comparison between the modeled and empirical acoustic responses shows that two of the three models can be confidently used to estimate pipe array acoustic responses. This study paves the way to the deconvolution of IMS infrasound data from pipe array responses and to the optimization of pipe array design to IMS applications.

### 1. Introduction

The infrasound component of the International Monitoring System (IMS) consists of 60 stations, of which 49 are already certified. Each of these stations is composed of an array of infrasound measurement systems capable of recording micropressure changes produced at ground level by the propagation of infrasonic waves. The primary objective of the IMS infrasound network is the detection of infrasonic waves directly or indirectly produced by nuclear explosions. However,

Corresponding author e-mail: Julien Marty, julien.marty@ctbto.org

data from this network have also demonstrated their value to a broad range of civil and scientific applications (Le Pichon et al. 2010). One of the main challenges of the infrasound technology is the high level of pressure background noise commonly observed at the ground level in the IMS frequency band (0.02–4 Hz). Since IMS infrasound stations are relatively sparse around the globe, signals of interest usually travel for thousands of kilometers through the earth's atmosphere before reaching the first IMS infrasound stations. The amplitude of these signals is therefore significantly attenuated before it is measured and usually relatively small compared to average background pressure fluctuations

produced at the ground by wind turbulence (Walker and Hedlin 2010). To observe signals of interest, it is therefore crucial to screen out as much as possible these pressure fluctuations produced by wind turbulence. This screening can be achieved through a combination of advanced measurement systems and signal processing techniques.

In the absence of wind turbulence, it is commonly assumed that the background noise of pressure fluctuations in the infrasound frequency band is mainly formed by a superposition of pressure fluctuations produced by the propagation of infrasonic waves coming from a broad range of local, regional, and global sources. This assumption is derived from the fact that coherent signals at a scale much larger than the size of wind turbulence structures can be generally observed in the entire IMS frequency band for extremely low wind conditions (Gabrielson 2011). This background noise of pressure fluctuations produced by a superposition of infrasonic waves is usually incoherent between the different elements of the same IMS infrasound station except in the (0.1–0.4 Hz) frequency band, which is also known as the microbarom band (Willis et al. 2004; Le Pichon et al. 2006), and in the  $(1-10\,\mathrm{Hz})$  frequency band, where local sources such as surf or man-made activities can regularly dominate the pressure fluctuation spectrum (Le Pichon et al. 2004; Garcés et al. 2006). When coherently detected by the different elements of the same IMS infrasound station, such waves are categorized at processing level in order to be distinguished from signals of interest. However, as soon as the wind speed increases, the background noise quickly rises well above these background noise pressure fluctuations produced by infrasonic waves and above the pressure fluctuations produced by most signals of interest. The reason is that wind-generated turbulence is by far the main source of noise in the infrasound frequency band (Christie and Campus 2010). Consequently, most efforts to reduce the pressure background noise target wind-generated noise.

The size of the spatial structure of wind turbulence is fortunately usually much smaller than that of infrasound wavelengths at similar frequencies (Mack and Flinn 1971; McDonald and Herrin 1975). Spatial averaging was therefore early identified as a very efficient technique to attenuate the amplitude of pressure fluctuations produced by wind turbulence while preserving the integrity of infrasound signals (McDonald and Douze 1971). To do so, spatial averaging must be performed on an area large enough compared to the size of wind turbulence but small enough compared to infrasound wavelengths of interest. Most of the developed solutions are mechanical systems in the form of a spatial distribution of air inlets linked together through a network of

pipes (Daniels 1959; Burridge 1971; Grover 1971; Hedlin et al. 2003; Alcoverro 2008) or in a form of wind protection structures (barriers, domes, covers, etc.) installed around the infrasound sensor (Hedlin and Raspet 2003; Shams et al. 2005; Christie and Campus 2010). While wind protection has proven its efficiency in reducing wind-generated noise, the size of the structures required to achieve acceptable noise reduction in the IMS frequency band and the sensitivity of the screening material response to environmental conditions are still obstacles to the implementation of these systems in operational conditions. The technical solution, implemented at all IMS infrasound stations, consists of a spatial distribution of air inlets linked to the infrasound sensor through a network of pipes. Such a system is commonly referred to as a "pipe array."

In the course of the progressive establishment of the IMS infrasound network, different pipe array designs have been implemented at IMS infrasound stations (Marty et al. 2012). An Infrasound Expert Group Meeting was organized in Jordan in 2011 to review the status of IMS wind noise reduction systems and to provide recommendations for optimizing pipe array design to IMS applications (Marty et al. 2011b). One of the main recommendations of this meeting was that the provisional technical secretariat (PTS) of the Preparatory Commission for the Comprehensive Nuclear-Test-Ban Treaty Organization (CTBTO) is provided with acoustic response models for pipe arrays. The objectives of this recommendation were manifold. The Infrasound Expert Group reported that the proper modeling of IMS pipe array responses would allow the assessment of the performance of existing pipe arrays, the improvement of pipe array design and the integration pipe array responses within overall infrasound system responses in order to improve the quality of data processing products.

The Infrasound Expert Group also suspected that a number of pipe array designs implemented at IMS infrasound stations had unstable phase responses, leading to different responses between the different measurement systems of the same infrasound station (Marty et al. 2011a). Since the infrasound automatic processing of the International Data Centre (IDC), located in Vienna, Austria, is based on array processing, unstable phase responses between the elements of the same array automatically lead to increased error in the computation of the wave parameters, if not to a nondetection (Marty et al. 2013; Brown et al. 2014). The Infrasound Expert Group therefore suggested performing a benchmark study across three distinct pipe array acoustic response models that were identified at the time of the meeting (Alcoverro and Le Pichon 2005;

Gabrielson 2013; Brown et al. 2014). It also recommended experimental validation of the models. The Infrasound Expert Group proposed to use a newly developed infrasound generator (Park et al. 2009) as a stable source of infrasonic waves.

The objective of this paper is to present the results of the comparison and validation of three acoustic response models for pipe arrays. The models and their characteristics are summarized in section 2. The models are then run for different pipe array configurations with the objective of highlighting the strengths and weaknesses of each model. The field experiment to validate the models is detailed in section 3. Section 4 presents the processing technique developed specifically for this experiment with the objective of optimizing the computation of acoustic responses to time periods with high signal-to-noise ratios (SNRs). Finally, the modeled and empirical acoustic responses obtained from the models and the field experiment, respectively, are compared in section 5.

## 2. Modeling

Two main concepts must be taken into account when modeling the acoustic response of a pipe array. The first one is the spatial distribution of the air inlets with the consequence that the input signal is generally not identical at all air inlets. The second one is the internal structure of the pipe array, which impacts acoustic signal propagation. Figure 1 summarizes these two general concepts. The input pressure signal p(t) arrives at each air inlet with a specific amplitude and time delay represented by the complex coefficients  $\alpha_k$ . It then propagates within the pipe array with each propagation path between an air inlet and the sensor measurement cavity being represented by the transfer function  $G_k(f)$ . The resulting output signal s(t) obtained in the sensor measurement cavity is composed of the sum of all these signals propagating within the pipe array.

The acoustic response models for pipe arrays developed by Alcoverro and Le Pichon (2005), Gabrielson (2013), and Brown et al. (2014) will be referred to as Models 1, 2, and 3, respectively, in the rest of the article. Model 1 is based on a complete electroacoustic description of the pipe array with electrical equivalents for all the system components, such as the air inlets, pipes, manifolds, and sensor cavities. The use of a dissipative transmission line model for pipes (Keefe 1984) allows the introduction of viscothermal losses and time propagation in the calculation. The system is then modeled as a linear system with multiple inputs (the air inlets) and one output (the sensor measurement cavity). For each input the transfer function is calculated in the

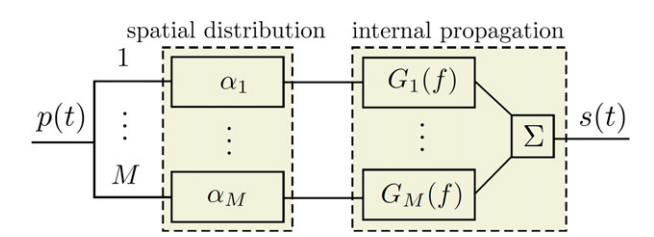


FIG. 1. Schematic diagram of pipe array acoustic response models.

frequency domain by connecting all other inputs to the ground. The spatial distribution of the wavefield is taken into account by introducing complex coefficients at all inputs. The overall response is then given by summing all elementary air inlet responses.

Model 2 also constructs the overall response by summing the individual air inlet responses. The air inlet transfer function is derived from a series of transfer matrices, each of them describing a system element through a corresponding admittance. One of the main differences between Model 1 and Model 2 is that Model 2 is based on local admittance rather than on a transmission line model with loss. It therefore uses the exact expression for the transition in circular pipes. Model 2 also takes into account adiabatic-to-isothermal transitions inside cavities and computes the air inlet transfer functions through the use of transfer matrices in lieu of loop and node analysis in the case of Model 1. It must be noted that Model 2 is the only one of the three models that was made available to the CTBTO Preparatory Commission. It was developed thanks to a voluntary contribution of the United States to the Preparatory Commission. The model is now available on demand to all CTBTO authorized users, such as national data centers and IMS station operators.

Finally, Model 3 considers the time delays resulting from the spatial distribution of the air inlets, and assumes an acoustic velocity that is dependent on the inner pipe diameter and signal frequency as described by Kirchoff's transmission line model. However, the remaining propagation effects within the pipe array structure are neglected. The input parameters of the three models are summarized in Fig. 2.

Figure 2 shows that all models take into account the spatial distribution of the air inlets. All models can also compute the system response for a specific wave azimuth and elevation angle. The spherical field and amplitude attenuation options included in Models 1 and 2 were developed for cases with nonplanar incident wavefields. It will be seen in section 3 that both these options were useful in the case of this study because of the nonplanar wavefield produced by the infrasound generator deployed during the field experiment. Models 1 and 2 also



FIG. 2. Features of Models 1, 2, and 3. Features displayed in light gray are not related to the acoustic response and will not be discussed in this study.

take into account the acoustic properties of all components of a pipe array, including air inlets, pipes, cavities, and resonance suppressors. Resonance suppressors are small devices that produce flatter resonances in pipe array frequency responses (Hedlin and Alcoverro 2005). Model 2 allows specifications of the air properties that can significantly impact the pipe array response for stations installed in extreme environmental conditions. Finally, Model 1 includes models for wind-generated turbulence and for simulating the efficiency of a pipe array in terms of noise reduction. These two model features will not be discussed in this paper because they do not relate to the acoustic response of pipe arrays. They are displayed in light gray in Fig. 2.

The acoustic response of pipe arrays usually takes the form of a high-order low-pass filter with multiple resonances toward the high-frequency part of the response. Since the acoustic response of the standard IMS 18-mdiameter configuration is, by design, close to unity in the entire IMS frequency band (0.02 Hz - 4 Hz), the use of such a configuration to compare and validate pipe array acoustic models would not be very instructive. It was therefore decided to define a set of six distinct configurations that would generate a certain number of resonances and damping effects in the infrasound frequency band. The objective of including different pipe array configurations in the comparison was to test the most critical model components independently. The number, length, and diameter of the system components with significant impact on the system response were therefore modified from one configuration to another. The dimensions of the components were also chosen in order to accommodate deployment as part of the field experiment, described in section 3. Figure 3 displays the general design of the default pipe array configuration used to validate acoustic response models. This configuration will be further referred to as "Config 1." Table 1 describes the length and diameter of the three pipes of

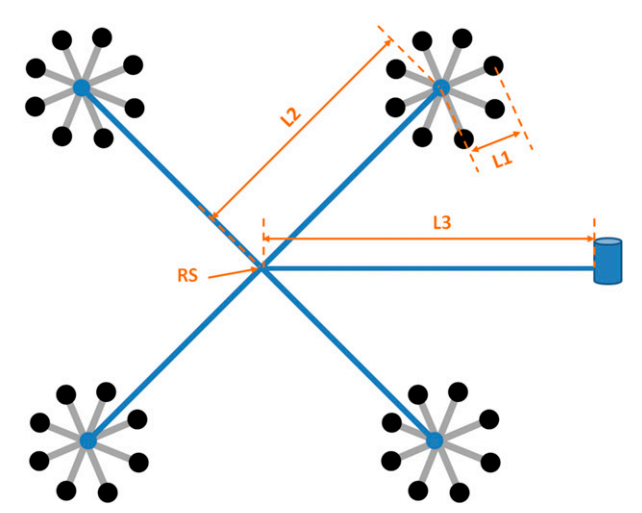


FIG. 3. Overview of default pipe array configuration used to validate acoustic response models (Config 1).

Config 1. Config 1 does not include any resonance suppressors (RS).

All five other pipe array configurations used to validate acoustic response models derive from Config 1. They will be referred to as Config 2 to Config 6. Only one component was changed between one configuration and another. The changes in characteristics for each configuration are described in Table 2. It can be seen that Config 2 does not include pipe L3. Config 3 and Config 4 are similar to Config 1 with the addition of a resonance suppressor in the manifold located at the center of the pipe array (Fig. 3). The difference between Config 3 and Config 4 is the diameter of the resonance suppressor: in the case of Config 3, it is adapted to the lowest frequency resonance of the system, whereas in the case of Config 4 it is not. Finally, Config 5 and Config 6 have a reduced diameter for pipes L2 and L3, and Config 6 includes an adapted resonance suppressor.

Figure 4 represents the acoustic responses of the six pipe array configurations to a planar and horizontal wavefield as computed by the three different models. The first striking observation when looking at all these responses is that Model 1 (dark blue) and Model 2 (purple) provide almost identical results. The phase responses in particular perfectly overlap. The second

TABLE 1. Length and diameter of Config 1 pipes.

Name	Length (m)	Diameter (mm)	
L1	3	15	
L2	15	15	
L3	20	15	

TABLE 2 Ch	nanges in char	actoristics b	atwaan Cor	nfig 2 6 and	Config 1
TABLE Z. CI	ianges in char	acteristics of	etween Coi	ang z-o and	Comig 1.

Name	L2 diameter (mm)	L3 diameter (mm)	L3 length (m)	RS diameter (mm)	RS length (mm)
Config 2	_	_	0 m	_	_
Config 3			_	2	50
Config 4				1.4	50
Config 5	8	8		_	_
Config 6	8	8		1.4	42

general observation is that the acoustic responses computed by Model 3 (light blue) are identical for the six pipe array configurations. This is because the spatial distribution of the air inlets is identical in the six configurations and because Model 3 neglects most propagation effects within the pipe array structure. The impact of the air inlet distribution is high with a zero at about 11.5 Hz, which can be clearly observed in the acoustic responses obtained from the three models and for all pipe array configurations. However, the acoustic responses obtained from Model 1 and Model 2 also display a number of resonances and damping effects with significant impact on the amplitude and phase responses. As seen in section 1, one of the primary objectives of this study is the proper modeling of IMS acoustic responses because of their impact on IDC data processing products. It appears that Model 3, which neglects most propagation effects within the pipe array, cannot be used to provide an accurate estimate of pipe array acoustic responses. The rest of the comparison and validation study will therefore focus on the results provided by Model 1 and Model 2.

Figure 4(1) displays a number of resonances, the first ones peaking around 2.7, 5.5, 10.5, 15.1, and 18.6 Hz. These resonances are mainly related to the length of pipes terminated by low impedance (air inlet or cavity). It can be seen in Fig. 4(2) that the first resonance is shifted toward higher frequencies because L3 is removed from the configuration. Figure 4(3) displays a similar amplitude response as Fig. 4(1) but without the first resonance. This is due to the resonance suppressor installed at the center of the pipe array. While the first resonance is removed, the phase response starts shifting around 0.2 Hz instead of 1 Hz in the case of Fig. 4(1).

The installation of resonance suppressors at IMS infrasound stations is still a controversial topic (Christie and Campus 2010). Some consider that resonances in the frequency response can affect the output of certain detection algorithms by favoring certain frequency bands in the detection. Since the background pressure fluctuation spectrum is generally not flat, detection algorithms are often applied on narrow frequency bands in any case. If the advantages of adding resonance

suppressors are minor, the drawbacks can be significant. The phase shifts associated with the use of such devices have two major consequences. First, since the phase shifts are not constant, the different frequency components of the same signal are shifted with different time delays. The form of the wave packet is therefore altered, leading to the misestimation of event magnitudes. Second, by introducing a device with such a small diameter, any minor partial obstruction of the device would significantly distort the response of the measurement system and lead to an increased error in the computation of wave parameters, if not to a nondetection (Alcoverro 2008; Marty et al. 2011a). This can be clearly seen in Fig. 4(4), which displays the acoustic response of Config 4. The only difference between Config 3 and 4 is the diameter of the resonance suppressor, which is reduced by 0.6 mm only. However, the acoustic responses of the two configurations are significantly different with a significant damping effect starting around 0.2 Hz as well as a phase shift starting around 0.05 Hz in case of Config 4. The use of a reduced diameter for the resonance suppressor indeed acts as an additional low-pass filter. This confirms the risk of significantly altering the system response and therefore data processing results when using resonance suppressors in operational conditions. A simple particle (moisture, dirt, humidity) with a diameter of a few tenths of a millimeter and stuck in the resonance suppressor would completely modify the overall system response. Such particles were found within some operational IMS pipe arrays, and the impact on the overall system response and on the results of the IDC automatic processing are clearly demonstrated (Marty et al. 2011b, 2013). For this reason, since 2012 resonance suppressors are not installed anymore at IMS infrasound stations. However, they remain at a number of historical IMS infrasound stations and are progressively removed as the stations are upgraded.

Figures 4(5) and 4(6) display the acoustic responses of Config 5 and Config 6, respectively. Both these configurations use 8-mm-diameter pipes for pipes L2 and L3 instead of 15 mm for the default configuration. This feature also acts as an additional low-pass filter, attenuating the resonance peaks and the rest of the

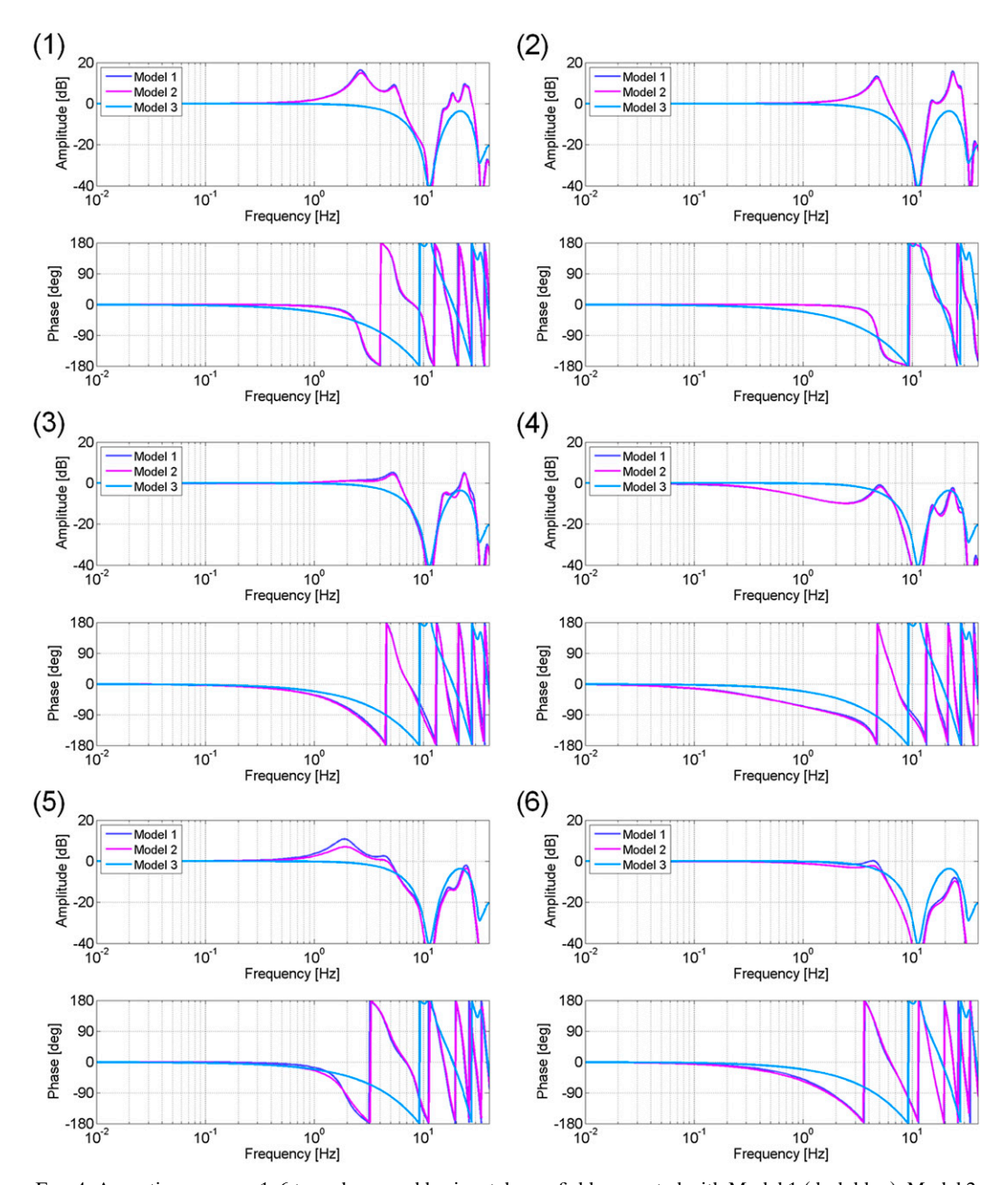


FIG. 4. Acoustic responses 1–6 to a planar and horizontal wavefield computed with Model 1 (dark blue), Model 2 (purple), and Model 3 (light blue) for Config 1–Config 6, respectively.

high-frequency part of the acoustic response. Figure 4(6) does not display the first resonance peak due to the use of a resonance suppressor in the center of the pipe array. To conclude, the six pipe array configurations clearly produce distinct acoustic responses. Models 1 and 2 providing extremely similar results for the six configurations; the next step of this study consists of comparing the modeled acoustic responses with empirical responses obtained through a series of field measurements.

# 3. Field experiment

As discussed in section 1, the background pressure fluctuations produced by wind-generated turbulence are by far the main source of noise in the infrasound frequency band. Pipe arrays are used to spatially average these background pressure fluctuations and improve the SNR for infrasound arrivals. To measure the response of pipe arrays to acoustic signal arrivals and not to wind turbulence, it is essential to work with infrasound signals

only. To do so, two methods were considered. The first method consists of using as a source the background pressure fluctuations recorded during time periods with extremely low wind conditions (Gabrielson 2011). As seen in section 1, acoustic signals are responsible for most of the background pressure fluctuations when wind turbulence vanishes. The second method involves using an infrasound generator. Neither of these two methods however relies on knowing the absolute source level. This is not realistic in case of the background pressure fluctuations, and the uncertainties around propagation effects would also make it difficult in the case of the signals produced by the infrasound generator. Both methods are in fact based on the comparison between the measurements of two parallel systems: an infrasound sensor linked to the pipe array under test and an open infrasound sensor installed at the center of the pipe array. The ratio of the two systems' responses therefore corresponds to the pipe array response provided that the input signal is purely acoustic.

To validate the pipe array acoustic models, a high SNR is required in the entire frequency band of interest. While the method based on background noise measurements for extremely low wind conditions can provide good results in some parts of the frequency band (Gabrielson 2011), it can require measurements over long time periods and does not always allow for the accurate estimation of the response at all frequencies. In addition, the level of the background pressure fluctuations for extremely low wind conditions can sometimes be below the self-noise of the MB2005 infrasound sensors used for this experiment, especially above 1 Hz (Christie and Campus 2010). Since a high SNR is required in the entire frequency band of interest, it was decided to use an infrasound generator to measure pipe array acoustic responses.

A broad range of low-frequency loudspeakers were produced over the last 30 years, some of them having the capability to project high-intensity infrasound to frequencies down to 10 Hz (Neill 1993). Recently, an alternative technology consisting of a baffled fan with dynamically controlled blade pitch was proposed by Park et al. (2009). This device, referred to as "rotary subwoofer," is capable of producing higher acoustic particle velocities than conventional transducers, which translate into higher radiated sound pressure levels. In order for the device to radiate as a simple source, the flow from the back side must be contained so that the acoustic radiation is only from the front side. This requires a substantial volume: the volume of the trailer is shown in Fig. 5. This volume is approximately  $9.14 \,\mathrm{m} \times 18.3 \,\mathrm{m} \times 4.3 \,\mathrm{m}$ . Only one prototype device set up at the Infrasound Laboratory of the University of



Fig. 5. Rotary subwoofer of the Infrasound Laboratory of the University of Hawai'i at Mānoa.

Hawai'i at Mānoa was available worldwide at the time of the experiment.

The experiment was carried out from 18 to 20 July 2012. All components of the six pipe array configurations were supplied by the Commissariat à l'énergie atomique et aux énergies alternatives (CEA), France. The air inlets, manifolds, and resonance suppressors were custom made for the experiment and stainless steel in construction. The pipes were industrial rubber hoses (Trelleborg 2016). The CEA also provided six sets of Martec MB2005 infrasound sensors and Nanometrics Taurus 24-bit digitizers. Whereas IMS infrasound data are usually sampled at 20 Hz, in the case of the field experiment it was decided to sample data at 100 Hz in order to measure more than the first two resonances of the pipe array acoustic responses. To protect the equipment from direct sun radiation, both the sensor and digitizers were covered with plastic boxes (Fig. 6).

The infrasound generator was initially deployed at about 150 m from the pipe array. At such a short distance from the source, it was anticipated that the wavefield could not be assumed to be planar. It was therefore decided to install five open reference systems across the pipe array to have the capability to estimate the shape of the wavefield. A reference system was installed at the center of each of the four rosettes and one was installed at the center of the pipe array. Each of the reference systems was composed of a MB2005 sensor linked to a single air inlet through a 10-cm-long pipe. The deployment of several reference sensors was also a good opportunity to improve the SNR by stacking the signals of the reference sensors and creating a virtual reference sensor.

Whereas the infrasound generator can generate monochromatic signals that can be detected at several



FIG. 6. Overview of the experiment setup. The pipe array is laid on the ground. Sensors and digitizers are covered by plastic boxes. The plastic boxes near the center of the array include power and communication system equipment.

kilometers with infrasound measurement systems, including pipe arrays (Park et al. 2009), the average pressure levels recorded by the open reference sensors during the experiment were most of the time above the amplitude of the signals produced by the infrasound generator in the initial setup. This was also because the wind velocity was quite high during the field experiment, leading to a high level of background pressure fluctuations. It was therefore decided to bring the generator closer to the pipe array at a distance of about 23 m from the center of the pipe array. We will see in section 4 that the source is modeled as a point source of spherical waves. The criterion for validity of this approach is the Rayleigh distance (Blackstock 2000), which is equal to the radiating area of the source divided by the acoustic wavelength. The point source approximation is valid for distances greater than the Rayleigh distance. In the case of this experiment, the Rayleigh distance did not exceed a few millimeters, which is at least three orders of magnitude smaller than the distance between the generator and the closest inlet port. Constructive and destructive acoustic interferences were also not considered in this study due to the very small distance between the air inlets and the ground in comparison with the wavelengths produced by the generator.

As for the signal shape, both monochromatic and swept-frequency cosine (chirp) signals were generated during the field experiment. While monochromatic signals allowed for the accurate computation of single-frequency points of the acoustic responses, the generation of 5-min chirps with a frequency ranging from 0.4 to 20 Hz proved to be a good time-quality compromise for estimating pipe array acoustic responses in the entire

frequency band of interest. For each pipe array configuration, 10 chirps were generated consecutively.

## 4. Processing technique

Figure 7 displays a schematic diagram of the field experiment. As in Fig. 1, p(t) represents the input signal,  $\alpha_{u,k}$  represents the complex coefficients associated with the spatial distribution of the wavefield, and  $G_{u,k}(f)$ represents the transfer functions of the paths between each air inlet and the sensor measurement cavity. The main difference between the diagrams for the pipe array acoustic models (Fig. 1) and the field experiment (Fig. 7) is that in the case of the field experiment, background noise pressure fluctuations  $w_{u,k}(t)$  are measured at each air inlet in addition to the acoustic input signal. The transfer function  $H_u(f)$  of the sensor and digitizer is also included and the resulting output signal writes  $x_u(t)$ . Subscripts u and r are used to differentiate whenever necessary the system under test (with pipe array) from the reference system, respectively. The coefficient associated with the wavefield spatial distribution writes  $\alpha_r$ , the transfer function of the small pipe and air inlet writes  $G_r(f)$ , the transfer function of the sensor and digitizer writes  $H_r(f)$  and the resulting output signal writes.

The objective of the field experiment is to measure the response of the different pipe array configurations to the acoustic signal produced by the infrasound generator through the comparison of the output signals  $x_u(t)$  and  $x_r(t)$ . To do so, it is necessary to make a number of assumptions. First, it is considered that the wavefield produced by the infrasound generator is perfectly circular around a single source point, which is the center of the rotary subwoofer, and that the amplitude of the wavefield decreases in 1/r, where r is the distance from the generator. This assumption derives from the characterization by Park et al. (2009) of the wavefield produced in near field by the infrasound generator up to  $16 \, \text{Hz}$ . It allows for computing all  $\alpha_{u,k}$  and  $\alpha_r$  coefficients.

The second assumption is that all background noise pressure fluctuations  $w_{u,k}(t)$  and  $w_r(t)$  are stationary processes with zero mean completely uncorrelated

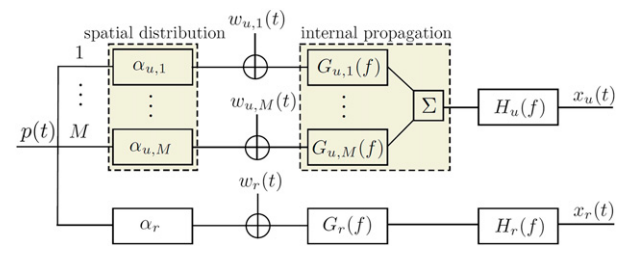


FIG. 7. Schematic diagram of the field experiment.

between each other and with the input signal p(t) produced by the infrasound generator. It could happen that  $w_{u,k}(t)$  and  $w_r(t)$  signals are correlated in the case of very low wind velocities because wind-generated turbulence would vanish and the background noise pressure fluctuations could be partially composed of acoustic signals. However, the experiment was carried out at a few meters from the seashore (Fig. 6), and the main source of pressure fluctuations was clearly wind-generated turbulence. This was verified by looking at the spectral levels of  $x_u(t)$  and  $x_r(t)$  before and after each acoustic sequence produced by the infrasound generator. Background noise pressure fluctuations  $w_{u,k}(t)$  and  $w_r(t)$ could also be found correlated in low frequency when the size of the turbulence becomes greater than that of the pipe array. For the purpose of this field experiment, it was decided to use a pipe array with a diameter (36 m) twice larger than that of the standard IMS pipe array diameter (18 m). With such a diameter it was estimated that wind turbulence could be seen as partially coherent over the scale of the pipe array below 0.2 Hz (Charbit et al. 2015). This was found acceptable, since the response of the pipe array at these frequencies is very close to unity and the field experiment was not tuned to the estimation of acoustic responses below 0.2 Hz in any case.

The transfer function  $G_r(f)$  was modeled and then measured during the experiment. It showed to be equal to unity up to 50 Hz and can therefore be removed from the system. The transfer functions of the sensors and digitizers  $H_u(f)$  and  $H_r(f)$  were also precisely measured in the laboratory before and after the field experiment. They were also estimated on-site just before starting the experiment. In addition, the MB2005 infrasound sensors used during the experiment are known for the stability of their response through time and their very limited sensitivity to environmental conditions (Marty et al. 2010; Ponceau and Bosca 2010; Hart et al. 2013). We can therefore confidently assume that the two transfer functions  $H_u(f)$  and  $H_r(f)$  were known at the time of the field experiment.

Now under these assumptions, if at any point in time the following condition is met

$$\gamma_{pp}(f) \gg \sum_{k=1}^{M} |\alpha_{u,k}|^{-2} \sigma_{u,k}(f),$$
(1)

then the acoustic response of the pipe array under test

$$G_{u}(f) = \sum_{k=1}^{M} \alpha_{u,k} G_{u,k}(f)$$
 (2)

can be uniquely determined from

$$G_{u}(f) = \frac{\gamma_{uu}(f)}{\gamma_{ur}(f)} \frac{H_{r}(f)}{H_{u}(f)}$$
(3)

with  $\gamma_{pp}$ ,  $\gamma_{uu}$ , and  $\sigma_{u,k}$  as the autospectra of p(t),  $x_u(t)$ , and  $w_{u,k}(t)$ , respectively; and  $\gamma_{ur}$  is the cross-spectrum between  $x_u(t)$  and  $x_r(t)$ . Condition (1) means that the amplitude of the background atmospheric pressure fluctuations recorded by the system under test must be negligible compared to the amplitude of the signal produced by the infrasound generator. While this would have been difficult to achieve with an open sensor, the noise reduction performed by the pipe array allowed for meeting this condition during the entire field experiment. This was verified by looking at the spectral levels of  $x_{\mu}(t)$  just before and during each test. Condition (1) was fulfilled during each of the tests but only around the central frequency (and harmonics) of the signal produced by the infrasound generator. Since chirps were produced by the infrasound generator, the signal central frequency varied through time. To identify the parts of the time-frequency space where condition (1) was met, the time-frequency space was split into small timefrequency windows.

The next step was then to identify the time-frequency windows for which condition (1) was met. To do so, one technique consists of looking at the coherence between signals  $x_u(t)$  and  $x_r(t)$ . This method proposed by Gabrielson (2011) is based on the fact that  $x_u(t)$  and  $x_r(t)$  are coherent in presence of acoustic signals but not in the presence of pressure fluctuations produced by wind turbulence. As discussed above, there are some limitations below 0.2 Hz due to the size of the wind turbulence relative to the size of the pipe array, but those do not apply to the frequency band of interest of this experiment. The computation of the coherence between signals  $x_u(t)$  and  $x_r(t)$  was therefore seen as a good mechanism to identify time-frequency windows with high SNRs.

Figure 8 represents the summary of the processing steps described above, including specific parameter values chosen for processing the data from the field experiment. The variables are replaced by their non-parametric estimates computed with Welch's (1967) method. The measured signals  $x_u(t)$  and  $x_r(t)$  are first sliced by time intervals i of 32-s duration with 75% overlap. The objective of this segmentation is to identify time–frequency windows with high SNRs. For each time interval i, the power spectral densities (PSD)  $\gamma_{uu,i}(f)$  and  $\gamma_{rr,i}(f)$  and the cross power spectral density (CPSD)  $\gamma_{uv,i}(f)$  of signals  $x_{u,i}(t)$  and  $x_{r,i}(t)$  are estimated using Hanning windows of 8-s duration and 75% overlap. PSD and CPSD calculations are then used to estimate the frequency response  $G_{u,i}(f)$  as per Eq. (3) and the

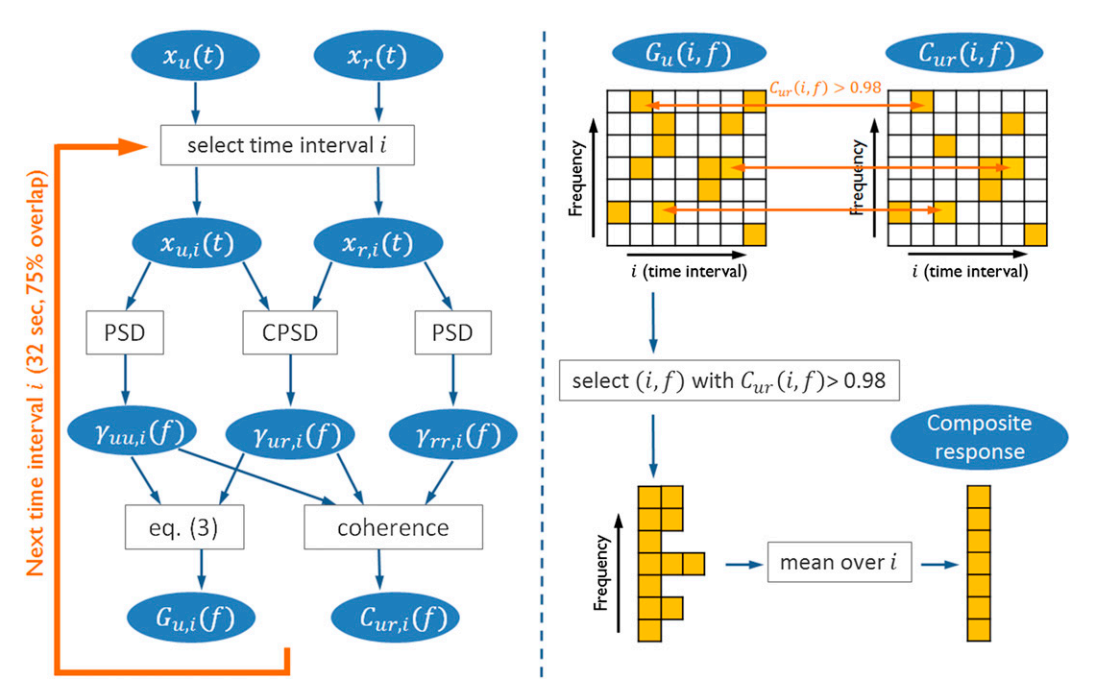


FIG. 8. Summary of the processing steps for estimating the acoustic response of the pipe array under test.

coherence  $C_{ur,i}(f)$  between signals  $x_{u,i}(t)$  and  $x_{r,i}(t)$ . Once frequency responses and coherence values are computed for all intervals i, indexes (i, f) for which  $C_{ur}(i, f) > 0.98$  are selected (displayed in orange in Fig. 8 matrices). The threshold of 0.98 typically allows for ensuring that condition (1) is met. The selected indexes are then used to identify time–frequency windows for which condition (1) is verified in the frequency response matrix  $\mathbf{G}_u(i, f)$ . These selected time–frequency windows are finally averaged over time in order to derive a composite response computed on windows with high SNRs only for the system under test.

# 5. Data analysis

Figure 9 represents the coherence matrix  $\mathbf{C}_{ur}(i, f)$  computed during the chirps produced by the infrasound generator. The chirps can be clearly seen in dark red because they correspond to a period of high SNR and therefore of high coherence. The chirp maximum frequency was 20 Hz. However, it can be seen that a number of high-frequency harmonics are also produced by the infrasound generator, allowing for identification of time–frequency windows with high SNRs up to 50 Hz. Below 0.8 Hz, the signal amplitude was not always high enough compared to background pressure fluctuations to reach a coherence level above 0.98 for each chirp iteration. This was the reason for generating a number of consecutive chirps. As a result, time–frequency windows

with a coherence level above 0.98 were identified for each frequency beam between 0.4 and 50 Hz and for each pipe array configuration.

Figure 10 represents the measured (green) and modeled (Model 1-blue, Model 2-purple) acoustic responses for the six pipe array configurations. The most striking observation is the near-perfect overlapping of the measured and modeled phase responses for the six configurations. Another general observation is that no zero appears in the pipe array response compared to the responses displayed Fig. 4. This is due to the nonplanar shape of the wavefield produced by the infrasound generator (Park et al. 2009) and to the use of a combination of sensors as reference to increase the SNR (see section 3). The measured amplitude responses also match very well the modeled ones for the six configurations. All resonances and damping effects are properly retrieved on both modeled and measured responses. A slight attenuation of the measured responses compared to the modeled ones can be observed beyond 20 Hz for Config 1-Config 4. This could be explained by several factors. First, the wavefield produced by the infrasound generator has not been characterized above 16 Hz and its shape could be different from the modeled one. Second, the wave amplitude attenuation factor with the distance could be slightly higher as the frequency increases.

A different damping effect that started around 2–4 Hz can be observed for Config 5 and Config 6. This

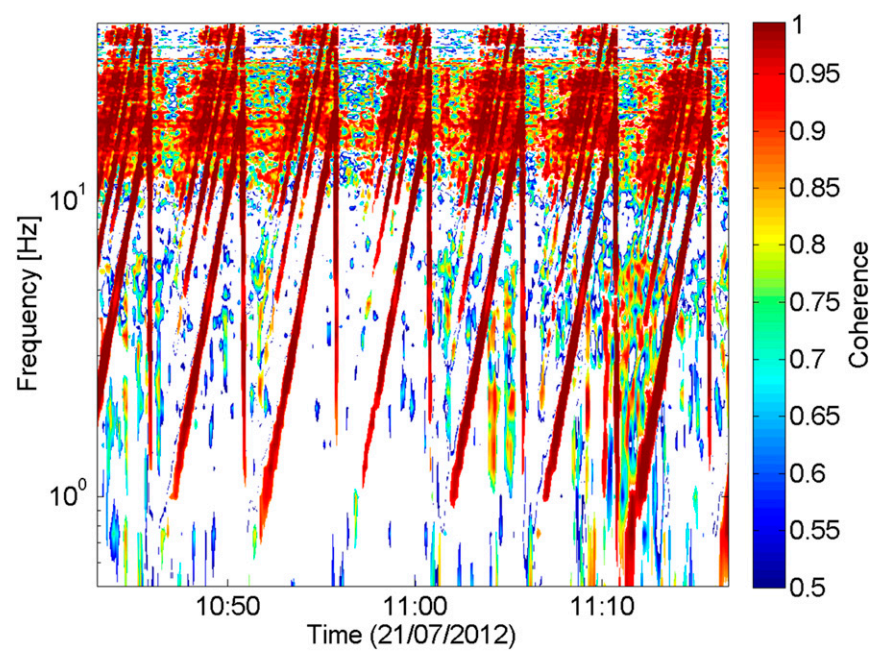


FIG. 9. Coherence matrix  $\mathbf{C}_{ur}(i, f)$  during chirps produced by the infrasound generator.

difference can most probably be explained by the extreme sensitivity of the pipe array response to pipe diameters below 10 mm. Reducing the L2 and L3 pipe diameters by a few tenths of millimeters would make the modeled and measured responses match perfectly. The sensitivity of the pipe array response to pipes with small diameters was already highlighted by Alcoverro (2008). For this reason, pipe arrays installed at IMS infrasound stations usually have a diameter greater than 13 mm and most of them are made of stainless steel or installed underground to limit thermal expansion. However, the pipes used for this temporary experiment were rubber hoses laid out directly on the ground with no protection from direct sun radiation. It is therefore probable that the pipe diameters slightly varied through the day. Since pipe diameters were not precisely measured at the time of the experiment, the diameter of 8 mm as provided by the manufacturer was kept in the models for the purpose of comparison. What can be learned from this experiment is the importance of using in operational stations pipes with a diameter large enough so as to not affect the pipe array response in the case of minor fluctuations of the pipe diameter. Despite these minor differences, the modeled and empirical responses are fitting almost perfectly together for all pipe array configurations. This demonstrates that Model 1 and Model 2 can be confidently used to estimate the acoustic response of pipe arrays in the infrasound frequency range.

### 6. Conclusions

In this paper the characteristics of three acoustic response models for wind noise reduction pipe arrays were described. The three models were then used to compute the acoustic responses of six distinct pipe array configurations. The results provided by two of the models were extremely similar. The third model however showed limited capabilities because of the nonconsideration of the main propagation effects within the pipe array structure. To validate the results provided by the two models in agreement, a field experiment was conducted. The measurements recorded by the system under test and the reference system were compared through a series of processing steps developed specifically for the purpose of this experiment. The modeled and measured acoustic responses appeared to fit extremely well for the six pipe array configurations. This showed that the models developed by Alcoverro and Le Pichon (2005) and Gabrielson (2013) can be confidently used to estimate the acoustic response of pipe arrays in the infrasound frequency band.

The modeling of the acoustic response of different pipe array configurations also allowed for highlighting the extreme sensitivity of the pipe array response to certain system components, such as resonance suppressors. The IDC infrasound automatic processing software being based on array processing is essential to ensure a stable phase response between all the measurement systems of the same infrasound array. The stability of

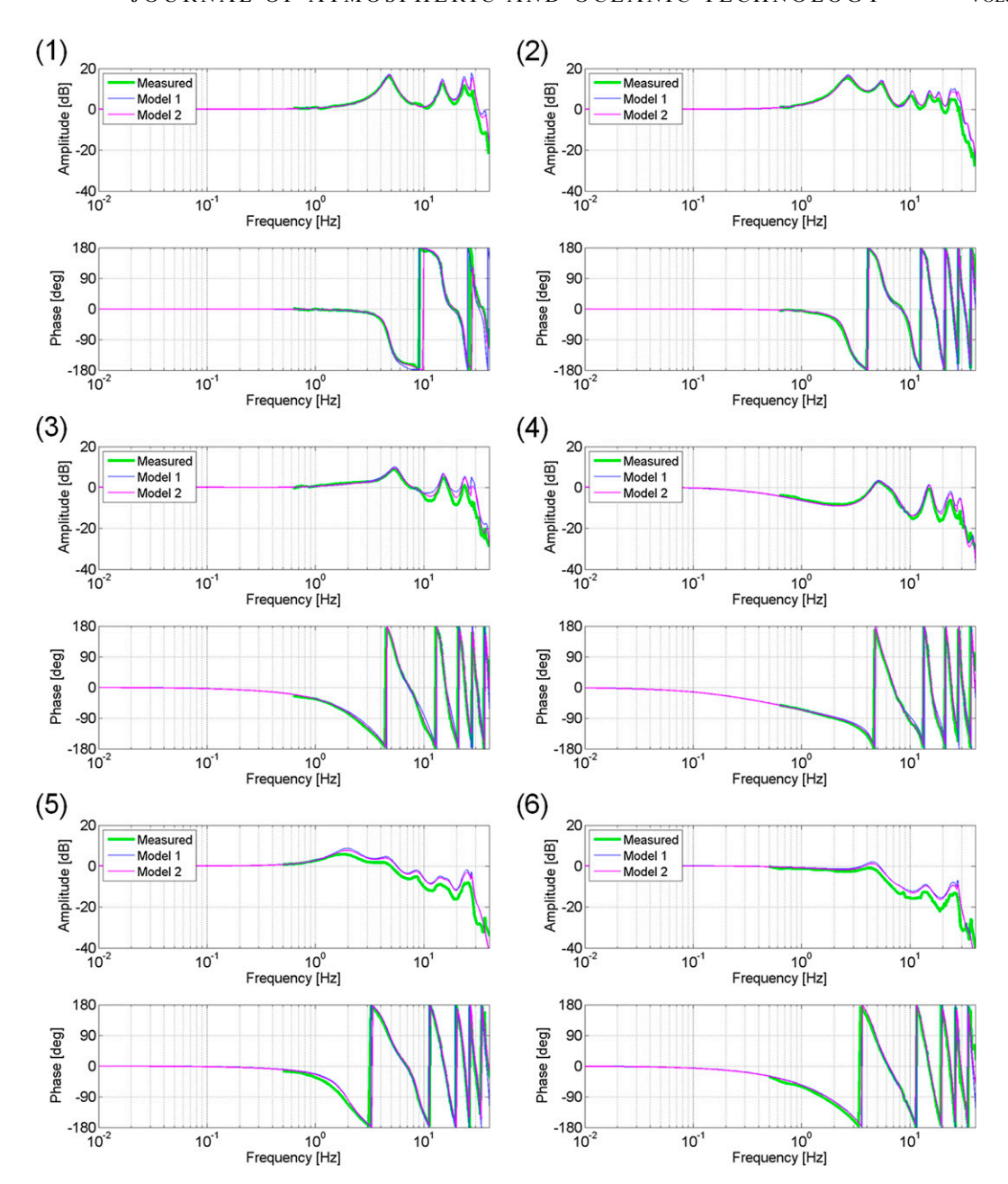


FIG. 10. Acoustic responses 1–6 measured (green) and modeled (Model 1—blue, Model 2—purple) for Config 1–Config 6, respectively.

the response of IMS sensors and digitizers is thoroughly tested before the equipment is approved for deployment in the IMS network and regularly verified through the life cycle of the equipment. However, it is much more difficult to control the acoustic response of the pipe array to ensure that it continuously remains within IMS requirements. To do so, several technical solutions were implemented since 2012. First, as the model developed by Gabrielson (2013) was made

available to the PTS, it has since then be used to optimize the design of IMS pipe arrays to detect infrasound signals in the (0.02 Hz – 4 Hz) frequency band. Second, the standard IMS pipe array design has evolved toward the use of more robust components and materials to ensure system stability through time. Third, a calibration capability was successfully implemented at the first IMS operational infrasound station in 2015 (Charbit et al. 2015; Kramer et al. 2015).

It allows for measuring on a regular basis the full frequency response of all the infrasound measurement systems installed at the station, including the pipe array. This capability is planned to be progressively rolled out through the IMS infrasound network.

The validation of acoustic response models for pipe arrays also paves the way to the integration of pipe array responses within IDC response files. The IMS data are available to all State Signatories and are provided together with response files for each channel of each station. However, up to now IDC response files only include sensor and digitizer responses for infrasound channels. Although the acoustic response of the new standard IMS pipe array system is close to one across the entire IMS frequency band, it departs from unity at higher frequencies. This information is of interest to the scientific community working on local infrasound sources and could be included in IDC response files. Furthermore, some historical IMS infrasound stations include pipe arrays with large diameter and nonflat acoustic responses in the IMS frequency band. The use of such a pipe array therefore has a significant impact on the output of the IDC automatic processing software. The issue with such historical systems is that the acoustic response of the pipe array significantly depends on the wave elevation angle, especially at high frequencies (Hedlin et al. 2003). If, for such systems, the pipe array response were added to IDC response files, it would have to be the response for a defined wave elevation angle, such as the averaged elevation angle for stratospheric arrivals. This would not provide accurate results for all arrivals but would already constitute an improvement from completely neglecting pipe array responses in the IDC automatic processing. It must be noted that, since 2012, these historical large diameter pipe arrays are progressively replaced with standard systems as they reach the end of their life cycle.

Finally, it must be noted that pipe arrays are not the only wind noise reduction systems present at IMS infrasound stations. These are often installed in combination with additional systems or environmental factors that help reduce wind-generated noise, whether they are man-made (gravel over air inlets) or natural (vegetation, snow, etc.). Some efforts have been made over the last few years to characterize the effects of such systems on noise reduction (Raspet and Webster 2015; Denis and Le Floch 2015), but their impact on acoustic signals has not up to now been thoroughly characterized. Future studies could, for example, consider optimizing gravel size and quantity over air inlets or ensuring that infrasound measurements are not significantly affected by certain snow conditions with the final objective of ensuring that IMS infrasound stations continuously fulfill IMS operational requirements and deliver highquality data.

Acknowledgments. The authors would like to express their gratitude to Prof. Maurice Charbit for the very useful comments. They would also like thank Mr. Jeremy Webster and Mr. Darren Hart for their support during the field experiment. The views expressed herein are those of the authors and do not necessarily reflect the views of the CTBTO Preparatory Commission.

#### REFERENCES

- Alcoverro, B., 2008: The design and performance of infrasound noise-reducing pipe arrays. *Handbook of Signal Processing in Acoustics*, D. Havelock, S. Kuwano, and M. Vorländer, Eds., Vol. 2, Springer, 1473–1486, doi:10.1007/978-0-387-30441-0\_80.
- —, and A. Le Pichon, 2005: Design and optimization of a noise reduction system for infrasonic measurements using elements with low acoustic impedance. *J. Acoust. Soc. Amer.*, **117**, 1717–1727, doi:10.1121/1.1804966.
- Blackstock, D. T., 2000: Fundamentals of Physical Acoustics. John Wiley & Sons, 568 pp.
- Brown, D., C. Szuberla, D. McComarck, and P. Mialle, 2014: The influence of spatial filters on infrasound array responses. *Pure Appl. Geophys.*, 171, 575–585, doi:10.1007/s00024-012-0586-1.
- Burridge, R., 1971: The acoustics of pipe arrays. *Geophys. J. Int.*, **26**, 53–69, doi:10.1111/j.1365-246X.1971.tb03382.x.
- Charbit, M., B. Doury, and J. Marty, 2015: Evaluation of infrasound in-situ calibration method on a 3-month measurement campaign. *Infrasound Technology Workshop 2015 (ITW2015)*, Vienna, Austria, CTBTO.
- Christie, D., and P. Campus, 2010: The IMS infrasound network: Design and establishment of infrasound stations. *Infrasound Monitoring for Atmospheric Studies*, A. Le Pichon, E. Blanc, and A. Hauchecorne, Eds., Springer, 29–75.
- Daniels, F., 1959: Noise-reducing line microphone for frequencies below 1 cps. *J. Acoust. Soc. Amer.*, **31**, 529–531, doi:10.1121/1.1907747.
- Denis, S., and C. Le Floch, 2015: Wind noise reduction systems: Complementary results. *Infrasound Technology Workshop* 2015 (ITW2015), Vienna, Austria, CTBTO.
- Gabrielson, T., 2011: *In situ* calibration of atmospheric-infrasound sensors including the effects of wind-noise-reduction pipe systems. *J. Acoust. Soc. Amer.*, **130**, 1154–1163, doi:10.1121/1.3613925.
- —, 2013: In-situ calibration of infrasound elements: Summary report (2009-2013). Nuclear Arms Control Treaty Tech. Rep., 84 pp.
- Garcés, M., J. Aucan, D. Fee, P. Caron, M. Merrifield, R. Gibson, J. Bhattacharyya, and S. Shah, 2006: Infrasound from large surf. *Geophys. Res. Lett.*, 33, L05611, doi:10.1029/ 2005GL025085.
- Grover, F., 1971: Experimental noise reducers for an active microbarograph array. *Geophys. J. Int.*, **26**, 41–52, doi:10.1111/j.1365-246X.1971.tb03381.x.
- Hart, D., R. Rembold, M. Hedlin, C. Coon, D. Szuberla, C. Fee, J. Helmericks, and J. Marty, 2013: IS56 Newport, WA component upgrade: Evaluation of the replaced digitizers (Geotech Dr24) and infrasound sensors (Martec MB2000) and implications for planning future maintenance and upgrades.

- Science and Technology Conf. (SNT2013), Vienna, Austria, CTBTO.
- Hedlin, M., and R. Raspet, 2003: Infrasonic wind-noise reduction by barriers and spatial filters. *J. Acoust. Soc. Amer.*, **114**, 1379–1386, doi:10.1121/1.1598198.
- —, and B. Alcoverro, 2005: The use of impedance matching capillaries for reducing resonance in rosette infrasonic spatial filters. *J. Acoust. Soc. Amer.*, **117**, 1880–1888, doi:10.1121/ 1.1760778.
- —, and G. D'Spain, 2003: Evaluation of rosette infrasonic noise-reducing spatial filters. *J. Acoust. Soc. Amer.*, **114**, 1807– 1820, doi:10.1121/1.1603763.
- Keefe, D. H., 1984: Acoustical wave propagation in cylindrical ducts: Transmission line parameter approximations for isothermal and nonisothermal boundary conditions. *J. Acoust.* Soc. Amer., 75, 58–62, doi:10.1121/1.390300.
- Kramer, A., B. Doury, J. Marty, and T. Grasse, 2015: Progress in the integration of on-site calibration capability at IMS stations: Towards measurement quality assurance. *Infrasound Technology Workshop 2015 (ITW2015)*, Vienna, Austria, CTBTO.
- Le Pichon, A., V. Maurer, D. Raymond, and O. Hyvernaud, 2004: Infrasound from ocean waves observed in Tahiti. *Geophys. Res. Lett.*, **31**, L19103, doi:10.1029/2004GL020676.
- —, L. Ceranna, M. Garcés, D. Drob, and C. Millet, 2006: On using infrasound from interacting ocean swells for global continuous measurements of winds and temperature in the stratosphere. *J. Geophys. Res.*, 111, D11106, doi:10.1029/2005JD006690.
- ——, E. Blanc, and A. Hauchecorne, Eds., 2010: Infrasound Monitoring for Atmospheric Studies. Springer, 735 pp., doi:10.1007/978-1-4020-9508-5.
- Mack, H., and E. Flinn, 1971: Analysis of the spatial coherence of short-period acoustic-gravity waves in the atmosphere. *Geophys. J. Int.*, 26, 255–269, doi:10.1111/j.1365-246X.1971.tb03399.x.
- Marty, J., D. Ponceau, and F. Dalaudier, 2010: Using the International Monitoring System infrasound network to study gravity waves. *Geophys. Res. Lett.*, 37, L19802, doi:10.1029/2010GL044181.
- ——, S. Denis, and M. Garcés, 2011a: Performance assessment of the IS07 infrasound station. *Infrasound Technology Workshop* 2011, Dead Sea, Jordan, CTBTO.
- ——, A. Le Pichon, and L. Evers, 2011b: IMS wind noise reduction systems. *Infrasound Expert Group Meeting 2011*, Dead Sea, Jordan, 6 pp.

- —, A. Kramer, and P. Polzer, 2012: IMS acoustic filtering systems. *Infrasound Technology Workshop 2012 (ITW2012)*, Daejon, South Korea, CTBTO.
- —, —, and P. Mialle, 2013: IS07 major upgrade. *Infrasound Technology Workshop 2013 (ITW2013)*, Vienna, Austria, CTBTO.
- McDonald, J., and E. Herrin, 1975: Properties of pressure fluctuations in an atmospheric boundary layer. *Bound.-Layer Meteor.*, 8, 419–436, doi:10.1007/BF02153561.
- —, E. J. Douze, and E. Herrin, 1971: The structure of atmospheric turbulence and its application to the design of pipe arrays. *Geophys. J. Int.*, 26, 99–109, doi:10.1111/j.1365-246X.1971.tb03385.x.
- Neill, P., 1993: Acoustical characteristics of a very low frequency sound source. M. S. thesis, Dept. of Physics, University of Mississippi, 100 pp.
- Park, J., M. Garcés, and B. Thigpen, 2009: The rotary subwoofer: A controllable infrasound source. J. Acoust. Soc. Amer., 125, 2006–2012, doi:10.1121/1.3082115.
- Ponceau, D., and L. Bosca, 2010: Low-noise broadband microbarometers. *Infrasound Monitoring for Atmospheric Studies*, A. Le Pichon, E. Blanc, and A. Hauchecorne, Eds., Springer, 119–140, doi:10.1007/978-1-4020-9508-5\_4.
- Raspet, R., and J. Webster, 2015: Wind noise under a pine tree canopy. J. Acoust. Soc. Amer., 137, 651–659, doi:10.1121/ 1.4906587.
- Shams, Q. A., A. J. Zuckerwar, and B. S. Sealey, 2005: Compact nonporous windscreen for infrasonic measurements. *J. Acoust. Soc. Amer.*, 118, 1335–1340, doi:10.1121/1.1992707.
- Trelleborg, 2016: Hydro'k manufacturing and machine tools. [Available online at http://www.trelleborg.com/en/apiv2/Download/ProductSheetPDF/8BD5976F-9081-4309-AE97-A90DA6A501C6.]
- Walker, K., and M. Hedlin, 2010: A review of wind-noise reduction methodologies. *Infrasound Monitoring for Atmospheric Studies*, A. Le Pichon, E. Blanc, and A. Hauchecorne, Eds., Springer, 141–182, doi:10.1007/978-1-4020-9508-5\_5.
- Welch, P. D., 1967: The use of fast Fourier transform for the estimation of power spectra: A method based on time-averaging over short, modified periodograms. *IEEE Trans. Audio Electroacoust.*, 15, 70–73, doi:10.1109/TAU.1967.1161901.
- Willis, M., M. Garcés, C. Hetzer, and S. Businger, 2004: Infrasonic observations of open ocean swells in the Pacific: Deciphering the song of the sea. *Geophys. Res. Lett.*, 31, L19303, doi:10.1029/2004GL020684.